PHILOSOPHICAL TRANSACTIONS OF THE ROYAL SOCIETY B BIOLOGICAL SCIENCES

The Wing Beat of Drosophila Melanogaster. I. Kinematics

J. M. Zanker

Phil. Trans. R. Soc. Lond. B 1990 **327**, 1-18
doi: 10.1098/rstb.1990.0040

Phil. Trans. R. Soc. Lond. B **327**, 1–18 (1990) [1]
Printed in Great Britain

THE WING BEAT OF *DROSOPHILA MELANOGASTER* I. KINEMATICS

By J. M. ZANKER
Max-Planck-Institut für biologische Kybernetik, Spemannstrasse 38, *D*-7400 *Tübingen, F.R.G.*

(*Communicated by M. F. Land, F.R.S. – Received* 26 *August* 1988)

CONTENTS

The wing beat of small insects attracts special interest because conventional aerodynamics predict a reduction of flight efficiency when aerofoils are small and slow. The kinematics of the wing beat of tethered flying *Drosophila melanogaster* were investigated by using artificial slow motion pictures which were generated by single strobe flashes triggered in synchrony with the wing beat. The properties of *Drosophila* wing motion are described qualitatively and compared with the published data for other dipteran insects. *Drosophila* moves its wings in a pattern that differs considerably from the well-documented wing beat of the bigger blowfly *Phormia*. By means of a computerized three-dimensional reconstruction, the variables of the wing-beat cycle, such as wing path and angles of attack, are analysed quantitatively. These data will be the basis of aerodynamic calculations presented in accompanying papers.

1. Introduction

Ever since man started watching nature, he has been fascinated by animal flight. Almost all behavioural components, such as migration, nutrition or mating, are observed to be airborne, in several classes of animals. Thus new ecological niches could be occupied by evolving the ability to fly. The actual flight technique and the corresponding design of a flying organism varies from the soaring of vultures with steadily spread wings to the hovering of tiny flies with rapidly oscillating wings.

Despite the manifold appearance of animal flight, science has tended to explain the underlying mechanisms according to a unifying principle of lift production. Simple empirical laws of aerodynamics describe the frictional and inertial interactions between the wings and the surrounding medium, as long as a sufficiently fast and large aerofoil is exposed to a steady air stream (for review, see Ellington (1984*a*)). However, for small flies two restrictions have to be taken into account. First, at low Reynolds numbers, i.e. for small and slowly moving aerofoils, the importance of frictional forces increases compared with that of inertial forces which induce lift at higher Reynolds numbers (Thom & Swart 1940; Horridge 1956). Here, friction could be employed for lift production, which would be reflected by certain kinematics ('swimming in the air'). Secondly, the air stream around the beating wings is by no means stationary, when the component of wing motion due to translational movements of the fly is small compared with the motion component due to wing oscillation. The extreme case is hoverflight at high wing beat frequencies, as observed in *Drosophila melanogaster* (Weis-Fogh 1973; Ellington 1984*a*). Thus the fruit fly appears to be an interesting model system for the investigation of the limits of flight capability.

An actively flying organism or machine has to solve two major problems. (i) It has to produce sufficient force to remain airborne and to counteract drag forces. (ii) It has to control these forces to stabilize flight. In *Drosophila*, for instance, changes of wing-beat amplitudes (Götz 1983) and postural changes of body appendages (Götz *et al.* 1979) can be combined into a simple feedback system that controls height, speed and course (David 1985; Zanker 1988). However, additional motor activity has to be assumed to account for an independent control of all six degrees of freedom of flight. Therefore, a closer look at wing-beat kinematics should reveal how wing motion is adapted to external stimuli, such as those experienced during disturbances.

To understand the basic mechanisms of *Drosophila* flight, the present study investigated both kinematics and dynamics of fixed flying *Drosophila melanogaster* wing beat. The results are presented in a series of three papers. Because our knowledge about the precise wing movements

in space is very limited, this paper (paper 1, Kinematics) contains an analysis of wing-beat kinematics during fixed flight in still air. The wing movements were reconstructed from artificial slow-motion pictures of tethered flying flies. Based on these three-dimensional data, the flight forces are calculated according to stationary aerodynamic theory. The calculated forces are compared with first attempts to measure the time course of the forces exerted by the fly in paper 2 (Dynamics, (Zanker & Götz 1990)). Finally, the changes of wing beat elicited by visual stimuli or in the wind tunnel are analysed in paper 3 (Control, (Zanker 1990)).

2. Materials and methods

(*a*) *Preparation*

In all experiments female wild-type *Drosophila melanogaster*, 3–8 day old, from the laboratory stock 'Berlin' were used. Under cold anaesthesia a steel pin was rigidly attached to head and thorax with dental cement (Scutan). By this pin the fly was glued to a stereo pickup and positioned in the centre of the experimental apparatus sketched in Figure 1*a*. The longitudinal body axis was kept horizontal, i.e. the average wing-stroke plane was about 50° inclined relative to the horizontal plane (Zanker 1988). Obviously, this is not the natural hovering flight posture, which would correspond to the experimental situation without external wind. In free hovering flight, the body axis is inclined roughly 60° relative to the horizontal plane (David 1978), i.e. the average stroke plane is about horizontal. This discrepancy between the present experiments and free-flight conditions seemed to be justified because measurements of the average flight force in *Drosophila* indicated no significant influence of the fly's orientation relative to gravity on the flight force production (Götz 1968). This led us to the assumption that, in a first approximation, kinematics should be independent of the actual body angle of the fly.

(*b*) *Artificial slow-motion pictures*

The piezo-type stereo pickup (ELAC PE 188) monitored the minute horizontal and vertical displacements of the fly during the wing-beat cycle. These displacements were small enough to create no motion blur in photographs, but produced an excellent signal:noise ratio in the piezo elements. The sinusoidal signal resulting from amplification and bandpass filtering of the pickup voltage was modulated with wing-beat frequency n_f and had a constant phase relative to the wing-beat cycle during stationary flight. It could therefore be used to synchronize single flashes of a strobe with the fly's wing beat.

The zero-crossings of this sinusoidal signal define an arbitrary beginning of the wing-beat cycle at time t_0, which corresponds to zero phase shift. The time T between two consecutive events t_0 is the inverse of the wing-beat frequency n_f. The period of the wing-beat cycle T is divided into k phase steps of duration Δt (usually $k = 25$). Single flashes of a strobe (TOURBO strobe 661) are triggered by a TTL pulse at the time $t_0 + i\Delta t$, with the relative phase shift i being an integer number between 1 and k. When i is held constant one observes a picture of the wings frozen in a fixed position depending on i, as long as the flight is stable. When i is periodically incremented between 1 and k, with an externally determined frame rate, an artificial slow-motion picture of the wing-beat cycle is generated. One should realize that this method gives only a time-averaged image of the wing beat, because successive pictures may be separated by several cycles. The strobe flashes can be synchronized to the external frame rates of various recording devices such as television or film cameras or an ordinary photographic camera. The

PHILOSOPHICAL TRANSACTIONS OF THE ROYAL SOCIETY B BIOLOGICAL SCIENCES

data presented here were collected with a 35 mm camera (Canon F1) at a frame rate of one exposure per second.

(*c*) *Spatial reconstruction*

For the spatial reconstruction, the wing of *Drosophila* is represented by six characteristic points on its surface, which can be easily localized in antidromic illumination as vein junctions. They are indicated by the circles in figure 1*b*. The three-dimensional reconstruction of a point requires at least two independent two-dimensional projections. To allow for two satisfying views of the surface of both wings at any time (i.e. any wing position), four projections of the fly were selected. They determined the mirror arrangement shown in Figure 1*a*: dorsal view, directly seen by the camera; laterodorsal view seen via mirror M_l; caudolateral view seen via mirror M_c; frontolateral view seen via mirror M_f. The fly is illuminated antidromically in all four projections by means of correspondingly adjusted light guides originating from the strobe.

For a given frame and a given wing the two projections providing the best view of the surface of the wing were chosen, and the head and abdomen tip and the six characteristic points on the wing were digitized (Summagraphics ID, VAX 750). The three-dimensional coordinates of the digitized points were reconstructed in space from the digitized points according to the method described in Appendix 2. At this level of the analysis the wing is represented as a three-dimensional polygon with an additional centre point. The comparison of the spatial

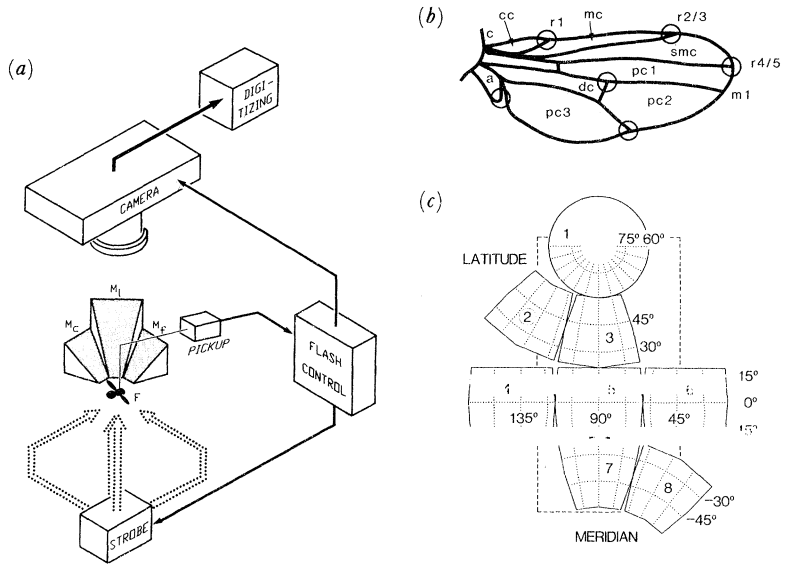

FIGURE 1. (*a*) Experimental apparatus. A tethered flying fly (F) glued to a stereo pickup is positioned in the centre of a set of mirrors (M_c caudolateral, M_l laterodorsal, M_f frontolateral). The fly is illuminated by four light-guide arms (indicated by dotted lines) originating from a strobe. The strobe flashes and the camera are controlled by the wing-synchronous signal from the pickup, thus generating artificial slow-motion pictures. The films were analysed frame by frame: six characteristic points of the wing surface were digitized on two of the four projections for computerized three-dimensional reconstruction. (*b*) Six characteristic points of *Drosophila* wing (marked by circles) defining the wing surface in the computer representation. c, costa; r 1–5, radius 1–5; m 1–4, media 1–4; cc, costal cell; mc, marginal cell; smc, submarginal cell; dc, discal cell; pc 1–3, posterior cell 1–3; a, alula. (*c*) Football projection. Eight adjacent sectors of the sphere surface are unfolded and projected vertically on the drawing plane. The latitudinal circles from 75° to −45° and the meridian circles from 30° to 150° are plotted on these patches with dotted lines in 15° distance. The broken lines indicate the region used for the presentation of the wing path in figure 8.

reconstruction of the wings with the actual photographs (see figure 2) demonstrates the reliability of the procedure. Extensive wing deformations, like those occurring when the two wings touch between upstroke and downstroke, are conserved in the primary sketches (see figure 2, phase step 11).

(*d*) *Wing-stroke variables*

A set of three orthogonal axes (longitudinal, transverse and vertical) was fitted to the six reconstructed points representing the wing surface in space. In a first step, a regression plane, defined by $z = c_0 - c_1 x + c_2 y$, was fitted to the six points $\boldsymbol{P}_i = (x_i, y_i, z_i)$. Thus position and inclination of the wing plane are reflected by its centre (average of all x_i, y_i, z_i) and the slopes in x- and y-direction given by c_1 and c_2. Note that two coordinates were treated as independent variables and one coordinate as a dependent variable by this procedure, although all three are equivalent, in reality. In the second step the points $\boldsymbol{P}_i$ are projected on the regression plane. The regression line to the resulting points $\boldsymbol{P}'_i$ represents the *longitudinal* axis of the wing; the line orthogonal to this regression line in the regression plane represents the *transverse* axis of the wing; the normal on the regression plane represents the *vertical* axis of the wing. By this simplifying procedure the wing is regarded as a flat plate and any information about wing deformations is lost.

To correct for small deviations of the fly's body axes from the coordinate system of the apparatus (due to imperfect adjustment), the complete data set of wing orientations was rotated until it was symmetrical for the left and right wings. This resulted in data all referring to a right-handed orthogonal body coordinate system. In addition, in most cases the data for both wings were pooled. The right wing's axis orientations were mirrored at the midsagittal plane and presented like the left wing's data. At this level of analysis the wing is represented by its average longitudinal, transverse and vertical axis, respectively. These variables were used for reasons of simplicity to calculate further kinematic and aerodynamic variables, such as wing orientation, velocity or angle of attack. A list of the used symbols of wing-stroke variables is provided in Appendix 1.

Whenever the time course of a wing-stroke variable is plotted in one of the present papers, the time t is given in non-dimensional fractions of the wing-beat period T. The mid-upstroke was arbitrarily chosen as time $t = 0$, because the corresponding wing posture is very simple to identify in all flight episodes. The non-dimensional time axis has the advantage that the data from the artificial slow motion pictures can be treated without further transformation, independent of the actual wing beat frequency n_f of an individual flight episode. Note, however, that to calculate the time derivatives of the wing position, such as velocities or accelerations, the frequency n_f recorded for the particular fly was taken into account. The average wing-beat frequency of the flight episodes presented here was 202 s^{-1} (± 2.8 s^{-1} s.e.m.).

(*e*) *Projection of wing-tip path*

The wing-tip path is represented by the unit vector of its longitudinal axis pointing to the surface of a sphere. It is impossible to develop the surface of a sphere on a flat plane without introducing distortions. In a parallel projection, for instance, the difference between a given distance on the surface and the corresponding distance in the projection increases with increasing eccentricity from the viewing axis. Several projections have been proposed which reduce distance or angular distortions for certain parts of the sphere. For the wing path of

Drosophila a lobed parallel projection was introduced, which was called a 'football projection' because it is similar to unfolding the patches of a football (for a more explicit discussion of the various possibilities to develop a spherical surface on a plane, see Zanker (1987)).

For the football projection (see figure 1*c*), the area of the sphere touched by the wing path is divided into 8 adjacent sectors with approximate diameters of 45°. The parallel projections of these fields are arranged in the drawing plane such that the clefts are small where the wing path crosses the border between different sectors. In this projection, angles and distances are well preserved, because in each individual sector the projectional distortions are smaller than 6% for a maximum eccentricity from the viewing axis of 20°.

(*f*) *Stimulation*

The experimental apparatus shown in figure 1*a* was designed as a compact block which could be installed in the open section of a wind tunnel or in front of an oscilloscope monitor which presented moving patterns to the fly. Thus various flight conditions could be simulated by well defined stimuli which elicit control responses of the fly (see paper 3).

3. Results

In the following, the wing-beat cycle is first described qualitatively. It is divided arbitrarily into four main phases with continuous transients: upstroke, dorsal reversal, downstroke and ventral reversal. This description is based on line drawings from original photographs showing the typical wing postures of the particular phase. For a better demonstration, projections were chosen here which could not be used for three-dimensional reconstruction. Thus the line drawings are compared with computer plots of the wing postures from another fly. Nevertheless, the quality of the computer reconstruction after the digitizing procedure can be roughly assessed on the basis of this comparison. The qualitative analysis is followed by a quantitative investigation of the wing-beat cycle. The shape of the wing tip path is scrutinized and its variability is discussed. Finally, the timecourse of kinematic wing-stroke variables is evaluated.

(*a*) *Upstroke*

During the upstroke the wings are elevated at very high speeds (figure 2*a–c*). The leading edge (costal vein) of the wing, which is directed backwards after the ventral reversal (see figure 2*l*), is now drawn upwards. The trailing edge (posterior cells) is dragged along like a flag. Sometimes the posterior cells can be observed swinging back (figure 2*b*) as if driven by inertial forces. In mid-upstroke the wings are extended along the transverse body axis with their spread oriented almost vertically (figure 2*a*). This posture can be identified very easily and was therefore used as phase step zero of kinematics. During the complete upstroke the wing is bent considerably between its base and its spread (black arrows in figure 2). Because only points on the wing spread were digitized, this bending is not preserved in the three-dimensional reconstruction (bottom rows in figure 2).

(*b*) *Dorsal reversal*

When changing from upstroke to downstroke, the wings reverse the direction of their translation and rotate about their longitudinal axis to reach their proper downstroke inclination (figure 2*d–g*). During the final upward motion the wings approach each other with

PHILOSOPHICAL TRANSACTIONS OF THE ROYAL SOCIETY B BIOLOGICAL SCIENCES

PHILOSOPHICAL TRANSACTIONS OF THE ROYAL SOCIETY B BIOLOGICAL SCIENCES

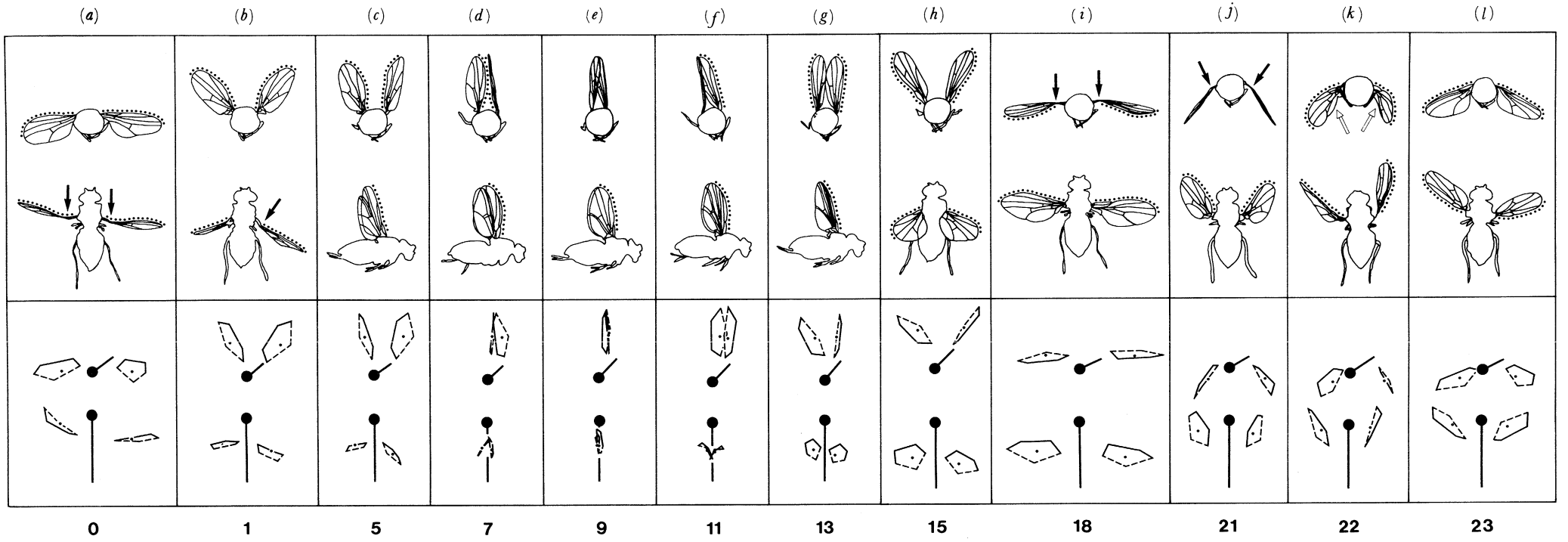

FIGURE 2. Wing-beat cycle. Line drawings (top) of a fly photographed in frontal projection, and dorsal (*a*, *b*, *h–l*) or lateral (*c–g*) view. The leading edge of the wing is marked by dots. Arrows point to the basal deflection of the wings. The computer reconstruction (bottom) depicts the wing posture in the same projections, but from a different fly. The body axis is given by a thick bar and the head is symbolized by a black dot. Because this fly was adjusted slightly obliquely relative to the external coordinate system, the fly's body axis does not disappear behind the head in the frontal view. The leading edge is plotted in continuous, the trailing edge in broken lines. The numbers denote the relative phase step in the wing-beat cycle. *Upstroke* (*a–c*). The wings are rapidly drawn from frontoventral to caudodorsal. Their inclination is almost vertical at the middle of upstroke. *Dorsal reversal* (*c–g*). The wings approach with their leading edges (*c*, 5) and touch each other. The area of contact increases, starting from the leading edges (*d*, 7) until the distal part of their spreads lie against each other (*e*, 9). Then they separate, starting from their leading edges again (*f*, 11) and begin to move downwards (*g*, 13). This sequence is called 'squeeze–peel'. Note that the dorsal view is possible in the computer reconstruction, although it cannot be seen directly in antidromic illumination. *Downstroke* (*h–j*). The wings move slowly from caudodorsal (*a*) to frontoventral (*b*). The leading edges are slightly lowered compared with the trailing edges. *Lower reversal* (*j–l*). When the wings are extended frontoventrally, the leading edges move from anterior (*j*) to posterior (*l*) whereas the trailing edges move from posterior (*j*) to anterior (*l*). This rotation appears to be extremely fast, because the intermediate position can be observed in very rare cases only. The best example, from another fly, is shown in (*k*). Note that during the quick rotation the wings are not fully synchronized and slightly rolled up (light arrows).

their leading edges (costal veins) moving dorsally and slightly frontally (figure 2*d*). The wings then touch each other, starting with their leading edges, and make contact on an increasing area of their spread until the wing spreads lie against each other (figure 2*e*). When the wings are peeled off again, starting with the costal veins, they are flexed along their transverse axis (figure 2*f*). Finally, they are separated completely and start moving downward (figure 2*g*).

A very similar process of attaching and detaching of the wings during the dorsal reversal phase of wing beat was first described in the small wasp *Encarsia formosa* and called 'clap–fling' (Weis-Fogh 1973). Because in *Drosophila* the wings are closed and opened like a flexible book, the modified form shown by this fly was called 'squeeze–peel' (Ellington 1984*c*; Götz 1987).

(*c*) *Downstroke*

During the downstroke (figure 2*h–j*) the wings move slowly to the anterior and ventral region. The frontal views of the fly show that the leading edges (costal veins) are slightly lowered compared with the trailing edges. During the complete downstroke the wing is bent downwards at its base (arrows in figure 2), which suggests some active flexion mechanism. In addition, in some cases the wing spread is cambered downwards(!), whereas in other cases it may behave like a flat plate (see figure 3*b*).

(*d*) *Ventral reversal*

At the end of the downstroke the wings are extended frontoventrally (figure 2*j*). The leading edge (costal vein) is situated anterior to the trailing edge (posterior cells). After a rapid rotation of the wing ('supination'), the leading edge lies posterior to the trailing edge (figure 2*l*), before the start of upstroke. Because the orientation of the wing's longitudinal axis scarcely changes throughout this process, the axis of rotation seems to lie behind the leading edge, somewhere on the wing spread.

Two observations indicate that this rotation is extremely fast. First, when the leading edge of the wing turns upwards from anterior to posterior (and slightly dorsal) and the trailing edge turns downwards from posterior to anterior, they must pass a situation where the leading edge is above to the trailing edge. However, in all artificial slow-motion pictures only wing positions before and after the rotation can be observed, but not the situation in between. The best approximation to the vertical wing posture – observed in a different fly – can be seen in figure 2*k*. Because the probability of observing this situation is apparently small, it must be very short in time. Secondly, closer inspection of figure 2*k* reveals that the leading edge of the right wing is still in an anterior position while that of the left wing is already in the posterior position. It is obvious that any lack of synchronization is best detected during the fast phases of wing beat. Cases of much stronger desynchronization, which might be associated with fatigue of the flies, can be seen in figure 3*a*.

(*e*) *Wing-tip path*

A first step to a quantitative description of wing beat is the investigation of the path of the wing. Two problems appear at this level of analysis. (i) The wing has to be represented by a set of variables that reflect its position and posture in space. The fitting of the longitudinal, transverse and vertical axes to the wing surface (explained above) is suitable for this objective. However, by this procedure the wings are consequently regarded as flat plates, which is only a crude approximation to reality. (ii) The wing path is best described by the unit vector of its

PHILOSOPHICAL TRANSACTIONS OF THE ROYAL SOCIETY B BIOLOGICAL SCIENCES

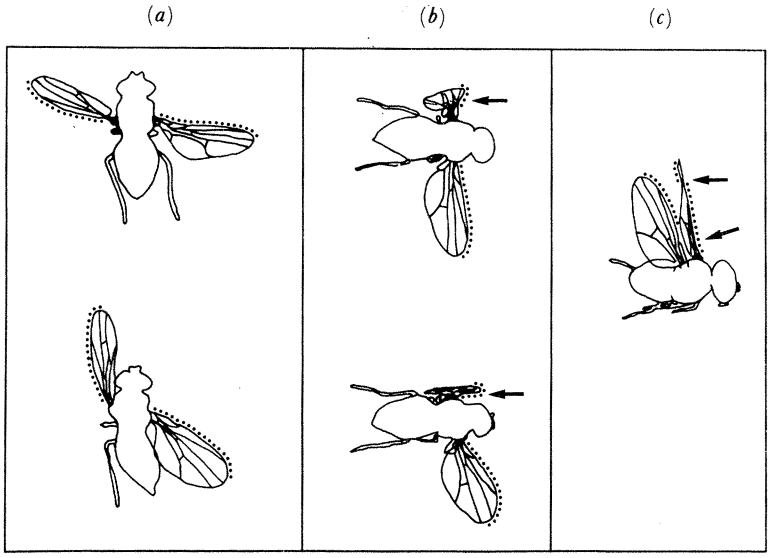

FIGURE 3. Peculiar wing postures. Line drawings as in figure 2, but from several flies in various projections. (*a*) Asynchrony between left and right wing at lower reversal in dorsal projection. The extreme case (bottom) is probably due to fatigue of the fly. (*b*) Different types of downstroke of a single fly in laterodorsal view. The wing may bend downwards (top) or behave like a flat plate (bottom). (*c*) Complex torsional deformations of the right wing (arrows) at the end of upstroke in frontolateral view.

longitudinal axis moving on the surface of a sphere. Here the difficulty arises of how to develop the spherical surface on a flat plane such as a sheet of paper. Projectional distortions increase with the size of the sphere's sector to be developed. Because the wings move across considerable parts of the sphere (the average wing-beat amplitude is about 135°) two methods were employed here to describe the wing path. First, the intersection points of the longitudinal axis with a unit sphere are plotted on the globe which can be seen in parallel projection from any desired direction. Second, the surface of the sphere is developed to the flat plane by using the football projection explained above (figure 1*c*), which reduces both angular and distance distortions.

The average paths of the left and right wings of 10 flies (1186 digitized frames) are plotted in figure 4*a* on globes, which are viewed from the side and from 30° above. The inclination of the transverse axis, as seen from the same point of view, is shown by the arrows associated with every second point. Both wings move on a narrow ellipsoid up–back and down–forward from a region near the dorsal pole of the globe to a region near the centre of the frontoventral part of the sphere. The upstroke is situated anterior relative to the downstroke.

Although the average picture of wing path does not differ significantly between the left and right wing, the path may vary considerably in individual flies. An extreme case is shown in figure 4*b* in the same projections as plotted in figure 4*a*. The path of the right wing is very similar to that of the average. However, the left wing moves on a rather irregular path with a completely different overall shape. It is not a narrow ellipsoid, but a figure-of-eight: the downstroke starts, as usual, posterior to the upstroke, but then crosses the upstroke path and moves anterior to it. The shape of the wing path has been the subject of an old controversy. For instance, Hollick (1940) observed figure-of-eight paths for *Musca* and *Muscina* in the wind, but ellipsoids as soon as the antennae were immobilized. In contrast, Nachtigall (1966)

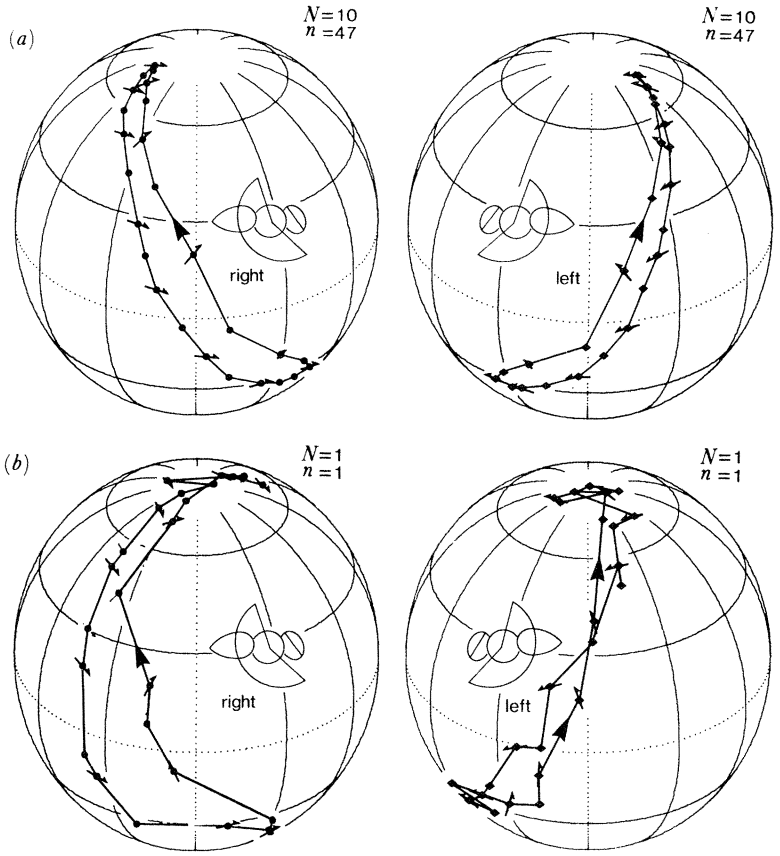

FIGURE 4. Wing path on globe. The angular positions of the right (dots) and left (diamonds) wing and their inclinations (arrows) are plotted on a sphere which is seen from lateral and from 30° above. (*a*) Average wing paths of 10 flies (1186 digitized frames, leading to about 47 values averaged at each phase step). Both wings move on narrow ellipsoids. The upstroke lies in front of the downstroke. (*b*) Example from a single fly for different wing paths of the left and right wing. The left wing does not describe an ellipsoid but a figure-of-eight with the upstroke crossing the downstroke.

described open ellipsoids in the wind and a closed path leading to paths similar to a figure-of-eight in still air for *Phormia regina*. A full discussion of these results is given by Zanker (1990), in comparison with the effects of wind on *Drosophila* wing path. For now, it should just be noted that the actual shape of the wing path might be of limited significance, because it is possible that an unstimulated fly moves its wings simultaneously on different paths on either side.

Despite the variability demonstrated here for the shape of the path, as a first approximation all data were averaged to allow for a rough characterization of the wing stroke. In figure 5 the average wing path, with the data of the left and right wing pooled in addition, is developed on the drawing plane according to the football projection explained above. From this plot, both the length of the travelled path and the angle of attack can be read immediately, because distance and angular distortions are minimized for the area of the sphere touched by the wing. The main features of wing stroke are: (i) The wing moves on a narrow, slightly flexed loop with the downstroke situated posterior to the upstroke. (ii) During the upstroke the leading edge is elevated relative to the trailing edge, ('nose up'), whereas the wings move slightly 'nose down' during the downstroke. (iii) The upstroke is much faster than the downstroke, as can be seen from the lower density of points on this part of the path (i.e. phase steps used for this part of the cycle).

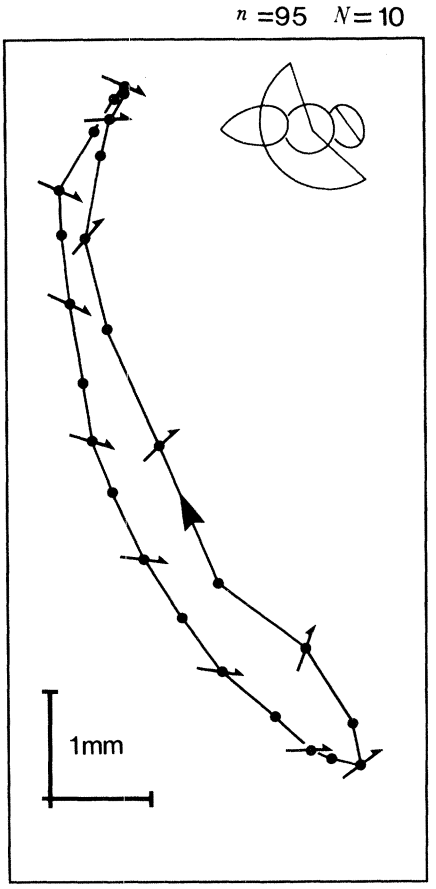

FIGURE 5. Average wing path of both wings in football projection (about 95 measures for each position). The arrows indicate the transverse axis of the wing; the leading edge (costal vein) is marked at its anatomical top side by the triangle. During the downstroke the wing moves slowly on the posterior part of the loop. The leading edge is lowered compared with the trailing edge. During the upstroke the wing moves fast on the anterior part of the loop. The inclination of the wing reaches high positive values.

(*f*) *Wing-stroke variables*

As next stage in the quantitative analysis of the wing beat, the timecourse of the essential wing beat variables was calculated. As long as the wing is regarded as a flat plate, the orientation and inclination of the wing can be represented by three angles. The two polar coordinates of the longitudinal wing axis in the body coordinate system, the meridian φ_l and the latitude θ_l are defined by the position of the wing on its path. The morphologic angle of attack α_m gives the inclination of the transverse wing axis to the body's horizontal plane, as seen from the direction to which the wing longitudinal axis points. Other kinematic variables can be deduced from these three angles, knowing morphological parameters, such as wing shape.

In figure 6*b* the average polar coordinates of the longitudinal axis, φ_l and θ_l, are plotted against time, showing how the wing moves back and forth and up and down (10 flies, 1186 digitized frames). In the figure no error bars are shown: the standard errors of the mean are too small to plot, owing to the comparatively high number of frames averaged in each of the 25 bins representing the different phases of the wing stroke (n ranges between 74 and 108; mean 95). The s.e.m. ranges between $\pm 1.6°$ and $\pm 4.0°$ (mean $\pm 2.7°$) for φ_l, and between $\pm 1.1°$ and $\pm 2.8°$ ($\pm 2.0°$ on average) for θ_l. The same set of data is plotted twice to facilitate

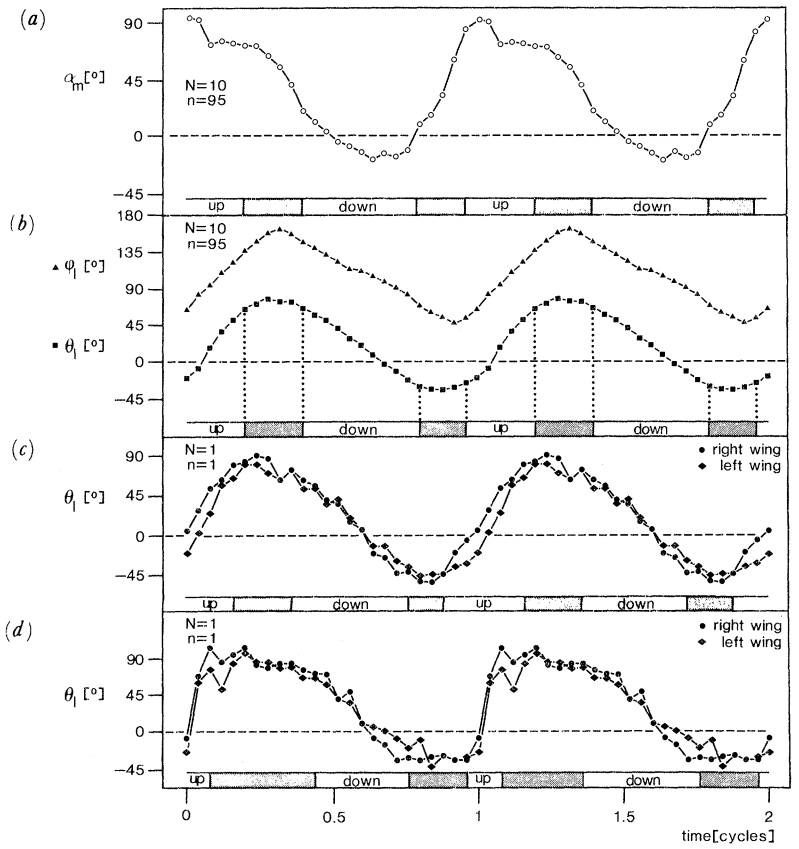

FIGURE 6. Time course of wing-stroke variables. The dimension of the timescale is given in fractions of the wing-beat cycle, divided in 25 steps. The same sets of data are plotted twice to facilitate the evaluation of the upstroke events. (*a*) Morphological angle of attack α_m. From $N = 10$ flies, 2×1186 wing postures were averaged in 25 phase step bins, leading to about $n = 95$ values per bin. The standard errors of the mean range between $\pm 2.0°$ and $\pm 7.6°$, with an average value of $\pm 4.1°$. The angle of attack increases during the lower reversal, is high during upstroke (nose up; see figure 5), continuously decreases during downstroke, and reaches small negative values (nose down; see figure 5). (*b*) Average polar coordinates of wing longitudinal axis (same data basis as in (*a*)). The standard errors of the mean range between $\pm 1.6°$ and $\pm 4.0°$ ($\pm 2.7°$ on average) for the meridian φ_l, and between $\pm 1.5°$ and $\pm 2.8°$ ($\pm 2.0°$ on average) for the latitude θ_l. The meridian φ_l (triangles) reflects the movement of the wings back and forth. The sawtooth-shaped curve indicates two different, roughly constant velocities in the equatorial plane. The latitude θ_l (squares) monitors the movements up and down with smooth accelerations during the reversals. The arbitrary borders of upstroke and downstroke are indicated by the vertical dotted lines. (*c*) Example of latitude θ_l of the wing longitudinal axis from a single fly. The slow upstroke is accompanied by a slight desynchronization between the left (diamonds) and right (dots) wing. (*d*) Example of latitude θ_l of the wing longitudinal axis from a single fly with an extremely fast upstroke.

the evaluation of the periodic behaviour. The φ_l curve has a triangular shape (i.e. almost constant forwards and backwards velocities), which implies acceleration peaks in the horizontal plane at the turning points. The course of θ_l more resembles a harmonic oscillation. The vertical dotted lines indicate how the cycle was divided arbitrarily into the four major wing beat cycle periods, upstroke ('up'), dorsal reversal (shaded), downstroke ('down') and lower reversal (shaded). This partition of the time axis is used further on as a rough 'event scale' of the wing-beat cycle.

The timecourse of either polar coordinate shows a considerable asymmetry between their slope of upstroke and downstroke, respectively. This was expected from the qualitative

examination,which has already shown that the downstroke takes much more time than the upstroke. The duration of upstroke may vary from fly to fly, as can be seen by comparison of figure 6*c* and *d*. In figure 6*c* the elevation θ_1 of the left and right wings of a single fly exhibits a slight desynchronization between the two wings during the very slow upstroke. The example of the most rapid upstroke is plotted in the same way in figure 6*d*. This fly needs only two phase steps to draw the wings from the lower reversal position to the upper reversal position.

The morphological angle of attack α_m is theinclination of the transverse wing axis to the parallel of latitude when looking in the direction of the longitudinal axis. As can be seen in figure 7*a*, α_m takes small negative values throughout the downstroke, i.e. the wing moves with the leading edge being slightly lowered. During the ventral reversal and the upstroke high positive values are achieved which correspond to the almost vertical orientation of the wing during upstroke (cf. figure 2).

4. Discussion

In the present paper, the average wing beat of *Drosophila* during stationary flight in still air was investigated by means of three-dimensional reconstructions of artificial slow motion pictures. After a short evaluation of the advantages and limitations of the used methods, the major features of the wing-beat cycle are summarized and compared with the data published for other fly species.

(*a*) *Artificial slow-motion pictures*

It is obvious that it is much simpler and cheaper to use a normal photographic camera and a strobe to generate artificial slow-motion pictures than to use elaborate and expensive high-speed cameras to shoot true slow-motion pictures. One has to bear in mind, however, that the wing beat is consequently represented in its time average; all transient changes are excluded. Two peculiarities of the artificial slow-motion pictures have to be discussed. (i) Zarnack (1981) noted that stroboscopic illumination might lead to phase ambiguities in the recorded sequences. This difficulty is overcome by triggering single flashes from the wing beat itself. Thus, a less ambiguous description of the wing-beat cycle is possible and latching of wing-beat frequency onto the strobe frequency is prevented. (ii) The correct sequence of phase steps is reproduced by the present method only if the flight signal triggering the strobe flashes is stable in time. If this is not the case (at the end of a longer flight episode, for instance) the phase of single exposures is shifted relative to the rest of the frames. Such 'phase jitter' is easy to detect, and the corresponding films were excluded from analysis.

A second major advantage of the present method is the possibility of analysing the wing beat on a non-dimensional timescale, which is independent of the actual wing-beat frequency. Owing to this data structure, the results from several flies can be averaged immediately. By the averaging procedure individual variations, which might be considerable (see figure 6*c*, *d*), are neglected. However, just as for the time average immanent to the method, it seems justified to look at the mean performance first, before analysing possible individual variations. The separate analysis of the single flight episodes led to the same basic results. This excludes strong deviations from the averages of the present study.

Another source of possible errors is introduced by the three-dimensional reconstruction of the wing from 'typical' points on its surface. Because all digitized points lie on the wing spread, the basal deflection of the wing observed in the photographs is not reproduced in the computer plots (see figure 2). In consequence, the longitudinal axes reconstructed from the points on the

PHILOSOPHICAL TRANSACTIONS OF THE ROYAL SOCIETY B BIOLOGICAL SCIENCES

wing spread may not coincide at the wing base. In addition, at the level of quantitative analysis, all wing-spread deformations were neglected because the wing is treated as a flat plate which is defined by its orientation vectors. However, again, for the first attempt to describe the wing beat quantitatively, the data may be reduced to the maximum simplicity. This seems justified because, for *Drosophila* flight, the actual shape and curvature of the wing seems to be of minor importance (Horridge 1946) owing to the low Reynolds number ($Re \approx 80$; for estimation, see Zanker & Götz (1990)).

(*b*) *Wing motion*

The wing-beat cycle was arbitrarily divided into four major periods. The upstroke (wings move from ventrofrontal to dorsocaudal) and the downstroke (wings move in opposite direction on a path slightly anterior to that of the upstroke) are separated by two reversal phases with comparatively complicated wing action.

During the dorsal reversal the wings touch each other with their spread like two halves of a flexible book which is closed and opened. This process was called 'squeeze–peel' (Ellington 1984*c*, Götz 1987) and was interpreted as an unsteady aerodynamic mechanism to improve the efficiency of lift production. By their reciprocal interference the two wings reduce the delay in the generation of circulation after wing acceleration ('Wagner effect'). Thus the complicated wing movements during the dorsal reversal may be very important for the continuity of flight force generation (Ellington 1984*c*; Lighthill 1973).

During the ventral reversal, the wings are extended ventrofrontally and then rotated. Because the leading edge moves from anterior to posterior and the trailing edge moves from posterior to anterior, the wing rotates approximately around its longitudinal axis. During this supination the wings' rotational velocity exceeds values of 10^5 deg s^{-1} (see figure 6*a*). Therefore one is tempted to call this process 'quick rotation'. It will be interesting to understand more about its various aspects of mechanics, neural control and aerodynamics.

(*c*) *Wing deformation*

In the quantitative analysis, the wings were treated as flat plates, because for the low Reynolds numbers of *Drosophila* the actual profile seems to be negligible for aerodynamic considerations (see above). Nevertheless it has to be noted that wing deformations can be observed throughout the complete wing-beat cycle. Three principal reasons may account for deformations of moving wings (Ennos 1987; Wootton 1981): (i) passive effects such as frictional, inertial or elastic forces; (ii) active mechanisms that put the wing under torsional tension (see, for example, Pfau 1978); (iii) aerodynamic forces, which attack eccentrically. It remains a matter of speculation, at the moment, which mechanism is responsible for which particular deformation of the wing surface. Moreover, we are far from completely understanding the aerodynamic effects of wing deformations. In the following, five major types of deformation of *Drosophila* wings are discussed briefly.

(i) During the whole wing-beat cycle the wing is bent at a point very near to its proximal end (see arrows in figures 2 and 3). This flexion might correspond to soft cuticular joints connecting the different parts of the costal vein. They are bent by the fly to a sharp angle during the cleaning of the wing, for instance. Active mechanisms seem to be responsible for this basal deflection of the wing because it appears to be independent of the variation of inertial and frictional forces during the wing-beat cycle. If the bending stress causing the basal deflection

PHILOSOPHICAL TRANSACTIONS OF THE ROYAL SOCIETY B BIOLOGICAL SCIENCES

can be controlled by the fly, the average stroke plane can be shifted relative to the fly's body. Such a shift is actually observed in wing-beat envelopes and was interpreted as a means of height and speed control (Zanker 1988). Here we find a possible candidate in wing-beat mechanics that could account for this control mechanism. (ii) Elastic or inertial forces might be responsible for the back-swinging of the wing spread during upstroke (figure 2*b*). (iii) During the quick rotation the wing is rolled up: the posterior cells of the wing are bent ventrocaudally when the costal veins are turned upwards backwards (light arrows in figure 2*k*). This might be due to inertial forces that delay the movement of the trailing edge, or to drag forces that reduce the motion of the trailing edge, which is the most flexible part of the wing spread. Of course, it is possible that the wing profile is controlled actively during the quick rotation by some of the steering muscles inserting at the wing base. (iv) Slight complex torsions of the wing can be observed at several phases of the wing-beat cycle (arrows in figure 3*c*). They cannot be explained in a simple manner and might result from any curious combination of the forces discussed so far. (v) A particular puzzle is the downwards flexion of the wing during downstroke, which cannot be attributed to inertial, frictional or aerodynamic forces (see figure 3*b*).

It was mentioned above that in comparison with the inertial forces which are responsible for life production at an aerofoil (Thom & Swart 1940), the frictional forces increase with decreasing Reynolds numbers. It was proposed that small flying animals could use the frictional forces in a sort of 'swimming in the air' instead (Horridge 1956; challenged by Ellington 1984*a*). In this case the wings should be spread out during the downstroke to push the air downwards, and drawn upwards with spreads bent towards the body to decrease friction during upstroke. The kinematics and especially the wing deformations reported here for *Drosophila* do not support such a hypothesis.

(*d*) *Dipteran wing-beat kinematics*

A first analysis of wing movements was done for *Drosophila virilis* (Vogel 1967). With single flash photographs it was demonstrated that the angle of attack is changed during downstroke when the fly is subjected to an airstream. The comparison of *Drosophila melanogaster* wing motion during courtship and fixed flight (Bennet-Clark & Ewing 1968) included a reconstruction of the wing path from multiple-exposure photographs. A new interpretation of wing-beat mechanics was based on the wing-tip path derived from high-speed films (Miyan & Ewing 1985). All photographs and wing paths published in these papers are in full agreement with the results presented here. None of these studies, however, covered all aspects of the three-dimensional reconstruction of wing beat from slow-motion pictures. Wing-beat kinematics in free flight were investigated for several other dipteran flies, such as *Tipula*, *Eristalis* and *Episyrphus* (Ellington 1984*b*). These wing paths and angles of attack, reconstructed from high-speed movies, served as a basis for elaborate aerodynamic and energetic calculations. The most extensive set of kinematic data was presented by Nachtigall (1966) for the tethered flight of the blowfly *Phormia regina*. These data are now compared with the data derived for *Drosophila melanogaster* here, to assess the similarities and peculiarities of the two species representing two size classes of flies.

The most striking difference between *Drosophila* and *Phormia* is that the two wings do not touch in the larger fly. Instead, in *Phormia*, the wings are less elevated during the dorsal reversal phase and are extended caudally with their anatomical bottom side looking upwards. From

PHILOSOPHICAL TRANSACTIONS OF THE ROYAL SOCIETY B BIOLOGICAL SCIENCES

this posture they rotate very fast to begin the downstroke with their top side dorsally. In contrast, in *Drosophila* the upper surface of the wing is seen in dorsal view both at the end of upstroke and at the beginning of downstroke. No fast rotation, but the slow squeeze–peel near to the pole is observed in between. The downstroke of *Phormia* starts on a shallow path and then is drawn steeply downwards, accompanied by a steady increase of the angle of attack. In *Drosophila* the wings first move downwards steeply and then shallowly with a corresponding decrease of the angle of attack. The rotation of the wing at the ventral reversal phase is much slower in *Phormia* than in *Drosophila*. In addition, the final inclination is less than vertical, i.e. the anatomical bottom side of the wing cannot be seen in dorsal view, as it can in *Drosophila*. Despite the smooth rotation, the wing deformation during that phase is much more pronounced in *Phormia*. During the upstroke, the deformation propagates distally over the wing spread like a torsional wave. During the final part of upstroke the inclination is increased such that the anatomical bottom side is seen in the dorsal view. In contrast, in *Drosophila* the wings are seen like flat vertical plates during the upstroke.

In summary, it has to be stressed that the wing-beat kinematics of *Drosophila* and *Phormia* differ considerably. The main peculiarities of *Drosophila* are the dorsal squeeze–peel and the ventral *quick rotation*. The downstroke and upstroke are adapted accordingly, to allow for these distinct reversal patterns. The aerodynamic implications of such differences will be discussed against the background of a closer view at the dynamic aspects of wing beat, gained in the second part of this study (Zanker & Götz 1990).

I thank K. Götz for all his support throughout the study. He, A. Borst, M. Egelhaaf and G. Mohn read and criticized earlier versions of the manuscript. B. Bochenek skilfully prepared the figures and helped with the evaluation of the experiments, and U. Flaiz typed the manuscript. Thanks are due to all of them. This work was supported by a grant from the M.P.G.

References

Bennet-Clark, H. C. & Ewing, A. W. 1968 The wing mechanism involved in the courtship of *Drosophila*. *J. exp. Biol.* **49**, 117–128.

David, C. T. 1978 The relationship between body angle and flight speed in free-flying *Drosophila*. *Physiol. Ent.* **3**, 191–195.

David, C. T. 1985 Visual control of the partition of flight force between lift and thrust in free-flying *Drosophila*. *Nature, Lond.* **313**, 48–50.

Ellington, C. P. 1984*a* The aerodynamics of hovering insect flight. I. The quasi-steady analysis. *Phil. Trans. R. Soc. Lond.* B **305**, 1–15.

Ellington, C. P. 1984*b* The aerodynamics of hovering insect flight. III. Kinematics. *Phil. Trans. R. Soc. Lond.* B **305**, 41–78.

Ellington, C. P. 1984*c* The aerodynamics of hovering insect flight. IV. Aerodynamic mechanisms. *Phil. Trans. R. Soc. Lond.* B **305**, 79–113.

Ennos, A. R. 1987 A comparative study of the flight mechanism of diptera. *J. exp. Biol.* **127**, 355–372.

Götz, K. G. 1968 Flight control in *Drosophila* by visual perception of motion. *Kybernetik* **4**, 199–208.

Götz, K. G. 1983 Bewegungssehen und Flugsteuerung bei der Fliege *Drosophila*. In *BIONA report 2* (ed. W. Nachtigall), pp. 21–34. Stuttgart: Fischer.

Götz, K. G. 1987 Course-control, metabolism and wing interference during ultralong tethered flight in *Drosophila melanogaster*. *J. exp. Biol.* **128**, 35–46.

Götz, K. G., Hengstenberg, B. & Biesinger, R. 1979 Optomotor control of wing beat and body posture in *Drosophila*. *Biol. Cybern.* **35**, 101–112.

Hollick, F. S. J. 1940 The flight of the dipterous fly *Muscina stabulans* Fallén. *Phil. Trans. R. Soc. Lond.* B **230**, 357–390.

Horridge, G. A. 1956 The flight of very small insects. *Nature, Lond.* **178**, 1334–1335.

Lighthill, M. J. 1973 On the Weis-Fogh mechanism of lift generation. *J. Fluid Mech.* **60**, 1–17.

PHILOSOPHICAL TRANSACTIONS OF THE ROYAL SOCIETY B BIOLOGICAL SCIENCES

Miyan, J. A. & Ewing, A. W. 1985 Is the 'click' mechanism of dipteran flight an artefact of CCl_4 anaesthesia? *J. exp. Biol.* **116**, 313–322.
Nachtigall, W. 1966 Die Kinematik der Schlagflügelbewegungen von Dipteren. Methodische und analytische Grundlagen zur Biophysik des Insektenflugs. *Z. vergl. Physiol.* **52**, 155–211.
Pfau, H. K. 1978 Funktionsanatomische Aspekte des Insektenflugs. *Zool. Jb. Anat.* **99**, 99–108.
Thom, A. & Swart, P. 1940 The forces on an aerofoil at very low speeds. *Jl R. Aeronaut. Soc.* **44**, 761–770.
Vogel, S. 1967 Flight in *Drosophila*. II. Variations in stroke parameters and wing contour. *J. exp. Biol.* **46**, 383–392.
Weis-Fogh, T. 1973 Quick estimates of flight fitness in hovering animals, including novel mechanisms for lift production. *J. exp. Biol.* **59**, 169–230.
Wootton, R. J. 1981 Support and deformability in insect wings. *J. Zool., Lond.* **193**, 447–468.
Zanker, J. M. 1987 Über die Flugkrafterzeugung der Fruchtfliege *Drosophila melanogaster*. Ph.D. disertation, University of Tübingen.
Zanker, J. M. 1988 On the mechanism of speed- and altitude-control in *Drosophila*. *Physiol. Ent.* **13**, 351–361.
Zanker, J. M. 1990 The wing beat of *Drosophila melanogaster*. III. Control. *Phil. Trans. R. Soc. Lond.* B **327**, 45–64. (This volume.)
Zanker, J. M. & Götz, K. G. 1990 The wing beat of *Drosophila melanogaster*. II. Dynamics. *Phil. Trans. R. Soc. Lond.* B **327**, 19–44. (Following paper.)
Zarnack, W. 1981 *Kinematische, aerodynamische und neurophysiologisch-funktions-morphologische Untersuchungen des Heuschreckenflug*. Göttingen: Habilitationsschrift.

Appendix 1. List of symbols

The following nomenclature of the symbols used in the three present papers is based on an orthogonal, right-handed, fly-centred coordinate system: the x axis points from caudal to frontal, the y axis points from right to left and the z-axis points from ventral to dorsal. All symbols are used according to the normal conventions of physics.

A_s	wing-stroke area
A_w	surface area of the wing
c	wing chord
C_D	coefficient of drag
C_L	coefficient of lift
D	drag force
d/u	ratio of duration of downstroke to upstroke
F_{ax}	horizontal component of aerodynamic force
F_{ay}	transverse component of aerodynamic force
F_{az}	vertical component of aerodynamic force
F_{ix}	horizontal component of inertial force of wing
F_{iy}	transverse component of inertial force of wing
F_{iz}	vertical component of inertial force of wing
F_s	force component normal to stroke plane
g	gravitational constant = 9.81 m s^{-2}
L	aerodynamic lift
m_{air}	mass of air accelerated by fly
m_{fly}	mass of fly
m_{wg}	total mass of wing
n_f	wing beat frequency
$\overline{P^*_a}$	mean specific aerodynamic power
$\overline{P^*_{acc}}$	mean specific power required to accelerate wing mass
$\overline{P^*_{ind}}$	mean specific induced power
$\overline{P^*_m}$	mean mechanical power output per unit mass of muscle
$\overline{P^*_{RF}}$	Rankine–Froude estimate of induced power per unit mass lifted
r	distance from wing base
r_G	distance of wing's centre of gravity from wing base
R	length of wing
Re	Reynolds number
t	time
t_0	time of beginning of wing beat cycle
Δ_t	time fraction of wingbeat period
T	period of wing beat cycle
v_a	aerodynamic effective velocity
v_{ind}	induced wind velocity
v_l	velocity component of air flow parallel to longitudinal wing axis
v_w	wind velocity in wind tunnel
v_x	horizontal velocity of wing, relative to far-field air
v_y	transverse velocity of wing, relative to far-field air
v_z	vertical velocity of wing, relative to far-field air
α_a	aerodynamic angle of attack: angle between transverse wing axis and velocity vector
α_m	morphological angle of attack: inclination relative to horizontal plane
γ	lift coefficient of rotational mechanisms
Γ_i	induced circulation
Γ_r	circulation of rotational movements
Γ_t	circulation of translational movements
η_a	aerodynamic efficiency of wingbeat
η_m	mechanochemical efficiency of wingbeat
φ_l	meridian of longitudinal wing axis
ν	kinematic viscosity of air = 1.46×10^{-5} m^2 s^{-1}
ρ	specific density of air = 1.29 kg m^{-3}
σ	spatial correction factor for wake inhomogeneity
τ	temporal correction factor for wake periodicity
θ_l	latitude of longitudinal wing axis

Appendix 2. Three-dimensional reconstruction

In a first step, the projection matrix was calculated for all four photographed images of the fly. The images were treated like parallel projections of the scene, because geometrical distortions of the camera setup were negligible. The projection matrix M describes the orientation of the particular view of the object space. To derive M, a '3D-cross' was photographed before every experiment, which consists of three intersecting perspex arms defining the three orthogonal axes of object space. The digitized tips of the three-dimensional cross represent the images of three unit vectors in the particular projection.

The image of a given point of object space represented by its vector $\boldsymbol{P}_i$ is given by the equation

$$\boldsymbol{P}'_i = sM\boldsymbol{P}_i. \tag{1}$$

$\boldsymbol{P}'_i = (x_i, y_i, z_i)$ is the transformation of the vector $\boldsymbol{P}_i$ in the image space defined by the projectional plane and its normal. The scaling factor s is the ratio of the distance between two given points in the object space to the distance of the projection of these points in the image space. The two components of $\boldsymbol{P}'_i$ in the projection plane, x_i and y_i, are determined directly by digitizing; the normal component z_i is calculated from the length L_i of $\boldsymbol{P}_i$ by

$$z_i = \sqrt{(L_i^2 - x_i^2 - y_i^2)}. \tag{2}$$

By digitizing the projections of the unit vectors $\boldsymbol{P}_1 = (1, 0, 0)$, $\boldsymbol{P}_2 = (0, 1, 0)$ and $\boldsymbol{P}_3 = (0, 0, 1)$, three vector equations of type (1) are given ($i = 1, 2, 3$). From this, one derives a very simple system of nine equations with the nine unknown elements of the projection matrix M, which can be rearranged to

$$M = \begin{bmatrix} x_1 & x_2 & x_3 \\ y_1 & y_2 & y_3 \\ z_1 & z_2 & z_3 \end{bmatrix}. \tag{3}$$

Any unknown point $\boldsymbol{P}$ digitized in two projections with the known transformation matrices M_A and M_B (leading to the image vectors $\boldsymbol{P}'_A$ and $\boldsymbol{P}'_B$) can now be transformed back to its three-dimensional coordinates in object space, $\boldsymbol{P} = (x, y, z)$. The two vector equations

$$\boldsymbol{P}'_A = sM_A\boldsymbol{P}, \tag{4a}$$

$$\boldsymbol{P}'_B = sM_B\boldsymbol{P}, \tag{4b}$$

derived from equation 1 can be rearranged line by line, leading to a system of six equations with five unknown factors: three coordinates in object space, x, y and z, and the two normal coordinates of each projection's image space, z_A and z_B. This overdetermined set of equations is reduced by selecting those equations which are most likely not to be hampered by digitizing errors (for a full description of that procedure see Zanker (1987)). Now the coordinates of the digitized point in object space, $\boldsymbol{P} = (x, y, z)$ can be calculated immediately by solving the remaining well-posed set of equations.

PHILOSOPHICAL TRANSACTIONS OF THE ROYAL SOCIETY B BIOLOGICAL SCIENCES